Properties of the Milky Way's Old Populations Based on Photometric Metallicities of the OGLE RR Lyrae Stars

P. Pietrukowicz[1], A. Udalski[1], I. Soszyński[1], D. M. Skowron[1], M. Wrona[1], M. K. Szymański[1], R. Poleski[1], K. Ulaczyk[1,2], S. Kozłowski[1], J. Skowron[1], P. Mróz[1,3], K. Rybicki[1], P. Iwanek[1], and M. Gromadzki[1]

[1] Astronomical Observatory, University of Warsaw, Al. Ujazdowskie 4, 00-478 Warszawa, Poland
e-mail: pietruk@astrouw.edu.pl
[2] Department of Physics, University of Warwick, Coventry CV4 7AL, UK
[3] Division of Physics, Mathematics, and Astronomy, California Institute of Technology, Pasadena, CA 91125, USA

ABSTRACT

We have used photometric data on almost 91 000 fundamental-mode RR Lyrae stars (type RRab) detected by the OGLE survey to investigate properties of old populations in the Milky Way. Based on their metallicity distributions, we demonstrate that the Galaxy is built from three distinct old components: halo, bulge, and disk. The distributions reach their maxima at approximately $[Fe/H]_{J95} = -1.2$, -1.0, and -0.6 dex on the Jurcsik's metallicity scale, respectively. We find that, very likely, the entire halo is formed from infalling dwarf galaxies. It is evident that halo stars penetrate the inner regions of the Galactic bulge. We estimate that about one-third of all RR Lyr stars within the bulge area belong in fact to the halo population. The whole old bulge is dominated by two populations, A and B, represented by a double sequence in the period–amplitude (Bailey) diagram. The boundary in iron abundance between the halo and the disk population is at about $[Fe/H]_{J95} = -0.8$ dex. Using *Gaia* DR2 for RRab stars in the disk area, we show that the observed dispersion of proper motions along the Galactic latitude decreases smoothly with the increasing metal content excluding a bump around $[Fe/H]_{J95} = -1.0$ dex.

Galaxy: bulge – Galaxy: disk – Galaxy: halo – Stars: variables: RR Lyrae

1 Introduction

Variable stars of RR Lyr type are pulsating yellow giants on the horizontal branch (Feuchtinger 1999, Marconi *et al.* 2015). Thanks to their relatively high luminosity (of about 50 $L_\odot$) and characteristic high-amplitude light curves, the variables are detected within the whole Local Group (*e.g.*, Martínez-Vázquez *et al.* 2016, 2017; Cusano *et al.* 2017). RR Lyr stars serve as standard candles and tracers of old populations (older than 10 Gyr). Thousands of variables of this type have been found in the Galactic bulge (*e.g.*, Soszyński *et al.* 2014), Galactic halo (*e.g.*, Torrealba *et al.* 2015), and halos of Local Group galaxies (*e.g.*, Sarajedini *et al.* 2012). The variables have been used in the determination of the distance to the Galactic center (*e.g.*, Pietrukowicz *et al.* 2015, Majaess *et al.* 2018) and numerous Galactic globular clusters (*e.g.*, Braga *et al.* 2015, 2016; Tsapras *et al.* 2017), also in the studies of the structure of the Milky Way (*e.g.*, Alcock *et al.* 1998, Pietrukowicz *et al.* 2012, Dékány *et al.* 2013, Zinn *et al.* 2014, Prudil *et al.* 2019) and Magellanic Clouds (Jacyszyn-Dobrzeniecka *et al.* 2017). RR Lyr stars as old objects provide important hints to the understanding

of the formation and early evolution of the Milky Way (*e.g.*, Kinemuchi *et al.* 2006, Szczygieł *et al.* 2009, Fiorentino *et al.* 2015, 2017, Belokurov *et al.* 2018).

Amongst the known RR Lyr variables there are fundamental-mode pulsators (RRab stars), first-overtone pulsators (RRc stars), and rarely observed classical and anomalous multiple-mode pulsators (RRd stars). RRab stars have several useful advantages over the other types. Variables of the RRab type have characteristic saw-tooth-shaped phase-folded light curves in the optical range. This significantly facilitates their proper classification in contrast to nearly sinusoidal RRc stars. Amplitudes of RRab stars are generally much higher than those of the other types. RRab stars get brighter than RRc stars with the increasing wavelength. These properties make the searches for RRab stars highly complete in the optical bands, in particular in the I band. At longer wavelengths, in near-infrared and mid-infrared, the amplitudes of the variables are smaller and the light curve shapes are more rounded, which hampers the detection and often leads to misclassification.

Finally, there is a very practical property of RRab stars that we use here. It is possible to assess metallicity [Fe/H] of the star based on its pulsation period and light curve shape. The method of estimating photometric metallicity was proposed by Kovács and Zsoldos (1995) and developed by Jurcsik and Kovács (1996).

In this work, we exploit the largest available homogeneous collection of RR Lyr stars, part of the OGLE Collection of Variable Stars*, to describe the Milky Way's ancient populations based on the information on photometric metallicity. The Optical Gravitational Lensing Experiment (OGLE) is a long-term variability survey conducted on the 1.3-m Warsaw telescope at the Las Campanas Observatory, Chile, of the Carnegie Institution for Science. Regular, high-quality OGLE observations (Udalski *et al.* 2015) of the Galactic bulge, Galactic disk, Small and Large Magellanic Clouds (SMC and LMC) have allowed the detection and classification of over 126 000 genuine RR Lyr stars amongst about one million variable objects of various types. Light curves of all OGLE periodic variables are inspected visually, which makes the collection pure and highly complete. The photometry is extracted with the help of image subtraction technique, especially suitable for crowded stellar fields (Woźniak 2000). Published time-series data contain hundreds to thousands of I-band measurements per star over at least two observing seasons. This guarantees well-sampled phase-folded light curves of RR Lyr variables, accurate determination of their pulsation periods, and the detection of possible amplitude and phase modulation, namely the presence of the Blazhko effect.

The latest releases of RR Lyr stars detected in the Magellanic System area and in the stripe of the Milky Way contain 47 828 and 78 350 objects and were published by Soszyński *et al.* (2019a) and Soszyński *et al.* (2019b), respectively. The analysis presented below is based on 56 424 RRab stars from the Galactic bulge/disk fields covering an area of 2750 square degrees and 34 229 RRab stars from the Magellanic System fields covering 765 square degrees.

2 Preparation of the samples

Proper analysis of the Milky Way's populations requires cleaning the RRab collection from members of Galactic globular clusters and members of nearby irregular galaxies. To clean our RRab samples from globular cluster stars, we

*http://www.astrouw.edu.pl/ogle/ogle4/OCVS/

used the updated catalog of variable stars in globular clusters† published by Clement *et al.* (2001). We cross-matched the catalog with the OGLE collection, verified each star individually, and noted only *bona fide* members and very likely members of the globular clusters. As a result, from the entire list of OGLE RRab stars observed in the Galactic stripe we removed 369 stars residing in 22 (mostly bulge) globular clusters. From the set of RRab stars observed in the Magellanic System area, we removed 18 variables from Galactic globular clusters 47 Tucanae and NGC 362 located in the foreground of the SMC.

To separate Galactic bulge from Sagittarius dwarf spheroidal (Sgr dSph) galaxy and to extract a Galactic halo sample from the background Magellanic Clouds, we applied simple brightness criteria. In Fig. 1, we present distributions of the mean I-band magnitudes of RRab variables from the entire Magellanic System area and a part of the Galactic bulge area containing the Sgr dSph core, where the applied magnitude boundaries are marked with vertical lines. The bulge part was cropped to $+10^\circ > l > 0^\circ$ and $b < -5^\circ$ after a series of experiments to check how far from the center of Sgr dSph the variables from this galaxy are detected. We found that, for instance, in the bulge area located on the opposite side of the Galactic center, for $l < 0^\circ$ and $b > +5^\circ$, there is no excess of detections around $I = 17.5$ mag in the brightness distribution. This magnitude limit was applied to variables detected in the shallow bulge survey, for which there is no V-band data so far. For variables from the regular OGLE-IV bulge survey (Soszyński *et al.* 2014) we used information on the $V-I$ color. We made exactly the same cuts in the color-magnitude diagram as shown in Pietrukowicz *et al.* (2015).

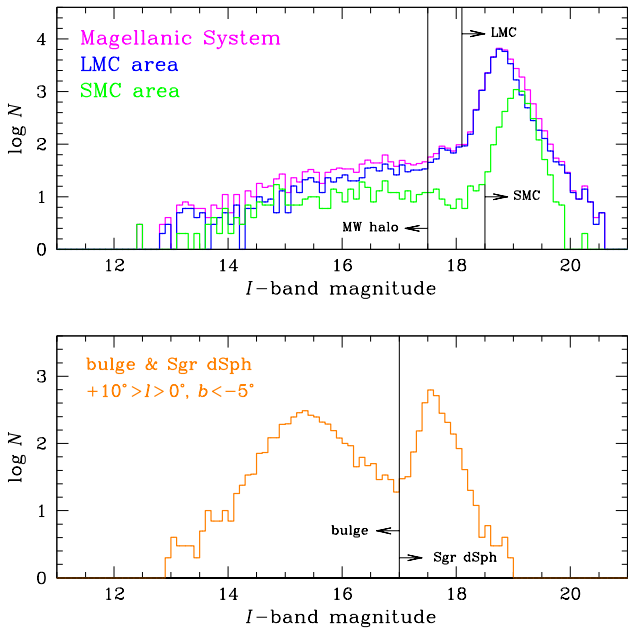

Fig. 1. Brightness distribution of OGLE RRab stars observed toward the Magellanic System (upper panel) and a selected bulge area with Sgr dSph galaxy in the background (lower panel). The following magnitude limits are used to select members of the nearby galaxies: $I = 18.1$ for the LMC, $I = 18.5$ for the SMC, and $I = 17.0$ for Sgr dSph. RRab stars observed toward the Magellanic System that are brighter than $I = 17.5$ mag belong to the Milky Way's halo.

†http://www.astro.utoronto.ca/∼cclement/read.html

As a result of the above operations, we extracted the following samples of RRab variables representing nearby galaxies: 2288 stars from the Sgr dSph, 26 947 stars from the LMC, and 4601 stars from the SMC. By fitting a straight line (power-law) to the brightness distribution on the far side of the bulge (for $15.5 > I > 17$ mag) and extrapolating it to fainter magnitudes, we estimate the contamination of the Sgr dSph sample by Milky Way stars at a level of 7%, or its purity of about 93%. The purity of the samples of more distant Magellanic Clouds is of about 97% assuming a constant level of contamination by halo stars in the brightness distribution. An estimated number of Sgr dSph variables left in the bulge sample is about 30. This is a negligible value for our analysis. To obtain a pure Galactic halo sample, we additionally removed RRab variables with I-band amplitudes below 0.2 mag located within a radius of 4° from the LMC center. Those are real but blended LMC objects, as it was noticed by Jacyszyn-Dobrzeniecka *et al.* (2017).

After the correction for globular cluster and Sgr dSph objects our final set of Galactic bulge and disk RRab stars contains 52 994 variables. The final halo sample contains 951 RRab stars. In total, 53 945 stars remained as representatives of the Milky Way's populations. Upper panels of Fig. 2 present the bulge area before and after the cleaning operation. Note that the area around the Sgr dSph center at Galactic coordinates $(l,b)=(+6°,-14°)$ seems to be free from stars from that galaxy. Lower panel of Fig. 2 shows the map of all RRab stars prepared for further analysis.

3 Metallicity Distributions

We estimate metallicities of the OGLE RRab stars using the following formula from Smolec (2005):

$$[\mathrm{Fe/H}]_{\mathrm{J95}} = -3.142 - 4.902P + 0.824\phi_{31}, \quad (1)$$

where P is the pulsation period and $\phi_{31}=\phi_3-3\phi_1$ is a Fourier phase combination for sine decomposition of the I-band light curve. The obtained metallicities are on the Jurcsik's (1995) scale (J95). The above formula was calibrated based on spectroscopic and photometric data for 28 RRab stars with iron abundances ranging from −1.7 to +0.1 dex and located in the Galactic field and two globular clusters. The formula provides a straightforward calculation of the metallicity using the I-band photometry. A weak point of this relation is its linearity and the lack of metal-poor stars for calibration. It is known to overestimate the iron abundance at the metal-poor end. According to Smolec (2005), the uncertainty of the relation is 0.18 dex.

We note that a more accurate, non-linear formula to calculate photometric metallicities was later proposed by Nemec *et al.* (2013) based on 34 RRab variables located in the original field of view of the *Kepler* space mission. The range of used metallicities is wider and spans from −2.6 to 0.0 dex. However, the formula from Nemec *et al.* (2013) in the application to the rich I-band OGLE measurements would require the use of additional transformations of the Fourier phase combination ϕ_{31} from the I-band to the V-band and from the V-band to the *Kepler* filter, provided for instance by Skowron *et al.* (2016) and Jeon *et al.* (2014), respectively. We found that these transformations generate a significant scatter making the metallicity distribution wider than expected on the metal-rich side. This is also in part due to the fact that the relation of Nemec *et al.* (2013) is calibrated only up to $[\mathrm{Fe/H}]=0.0$ dex, which, combined with its

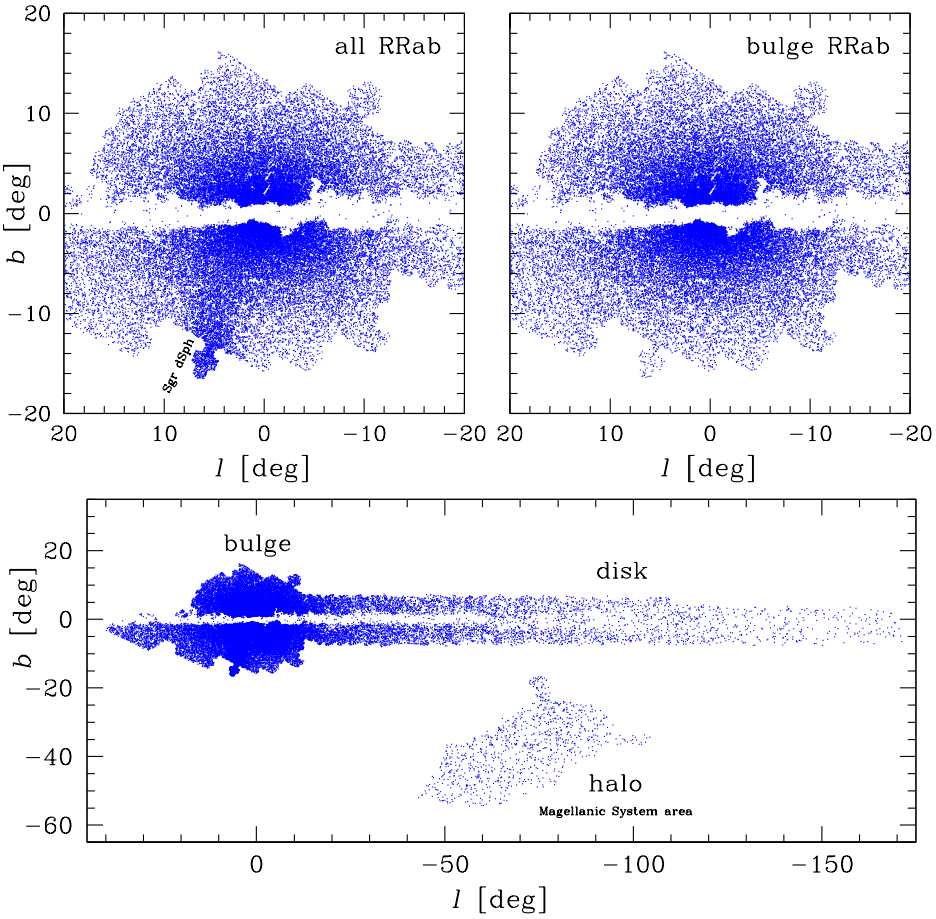

Fig. 2. Upper left panel: distribution of OGLE RRab variables detected toward the Galactic bulge. Upper right panel: the sample cleaned for globular cluster members and stars from Sgr dSph galaxy. Lower panel: distribution of 53 945 only-Galactic RRab variables observed in all OGLE fields covering about 3515 square degrees of the sky. Due to extreme extinction along the Galactic plane, many stars in this region are not visible in the optical range.

non-linear dependence on ϕ_{31}, may overestimate the photometric metallicity at the metal-rich end. Since the majority of bulge RRab fall within a calibration region of the relation of Smolec (2005), we decide to use this relation in our study.

In Fig. 3, we present metallicity distributions for various sections of the Milky Way and for nearby irregular galaxies. In the upper panel of this figure, we compare distributions for inner bulge (stars observed within the angular radius $r = 10^\circ$ from the origin of the Galactic coordinates), outer bulge (stars with $10^\circ < r \leq 20^\circ$), bulge-to-disk transition area ($20^\circ < r \leq 30^\circ$), disk area ($r > 30^\circ$), and for the Galactic halo sample extracted from the Magellanic System fields. Both bulge distributions show a sharp peak at $[\mathrm{Fe/H}]_{\mathrm{J95}} \approx -1.0$ dex. This peak is less prominent in the bulge-to-disk transition region. In the disk area, there are two maxima at different iron abundance, a larger one at $[\mathrm{Fe/H}]_{\mathrm{J95}} \approx -1.2$ dex and a smaller one at $[\mathrm{Fe/H}]_{\mathrm{J95}} = -0.6$ dex. The shape of the pure halo population allows us to explain the mentioned distributions. The metal-poor sides of all distributions are very similar to each other—they have the convex shape of the halo distribution. This means that the halo population is present in all parts

of the Milky Way including its inner regions. The larger of the two maxima in the disk area (at $[\mathrm{Fe/H}]_{\mathrm{J95}} \approx -1.2$ dex) corresponds to the halo distribution. The metal-rich component certainly belongs to the old disk population as this component is not seen at high Galactic latitudes.

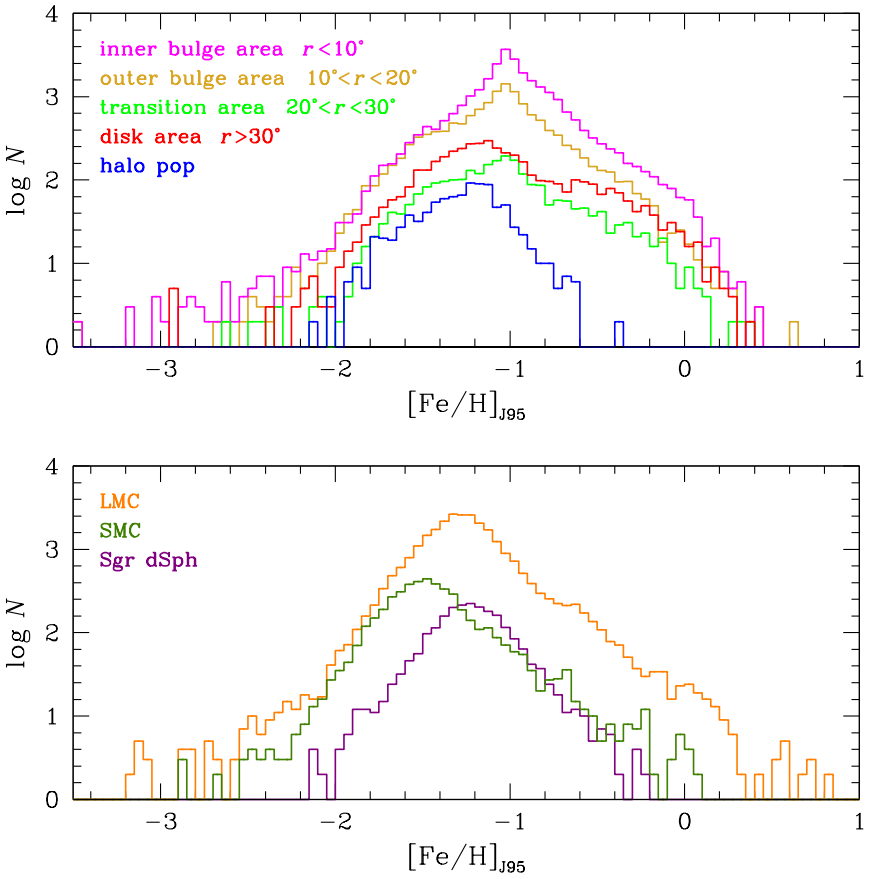

Fig. 3. Metallicity distributions for RRab stars observed in various directions in the Milky Way (upper panel) and in nearby galaxies (lower panel). Note a very similar, convex shape of the metal-poor side of the distributions in all directions indicating that the halo penetrates down to the very central regions of the Galactic bulge. The distribution for the disk area has two maxima, a metal-poor one corresponding to the Galactic halo population and a metal-rich one corresponding to the old (thick) disk population.

We note here that foreground disk stars contribute insignificantly to our bulge sample. There is no sharp boarder between the disk and the bulge. However, we can safely assume that RR Lyr stars observed toward the Galactic bulge and located closer than 3 kpc from the Sun do not belong to the bulge. Approximately, at that distance we can find globular cluster M22 (3.1 ± 0.2 kpc, Kunder *et al.* 2013). Only 55 RRab variables from the bulge area have the mean brightness $I < 13.1$ mag or are brighter than RR Lyr stars from M22. This low number of bright stars in the sample also stems from the saturation limit in the OGLE regular bulge survey of $I \approx 12.5$ mag. The mentioned 55 RRab stars may belong to the disk as well as to the halo population. Therefore, we decided not to apply any cuts for bright variables from the bulge fields in the cleaning process.

In Fig. 4, we try to estimate what fraction of halo RR Lyr stars is present in the bulge. We scaled the halo profile and subtracted it from the bulge profile. The scaling factor was found by minimizing the difference between the two profiles for $[\mathrm{Fe/H}]_{\mathrm{J95}} \leq -1.4$ dex. It turns out that within $r = 20^\circ$ from the center about 32% of the RR Lyr stars are halo interlopers. For $r < 10^\circ$ and $r < 5^\circ$ we obtained 25% and 19%, respectively. This is consistent with a very recent result by Kunder *et al.* (2020). Their spectroscopic survey of 2768 RRab variables in the area $+8^\circ > l > -8^\circ$ and $-6^\circ < b < -3^\circ$ showed that 25% of the sample stars belongs to the halo population.

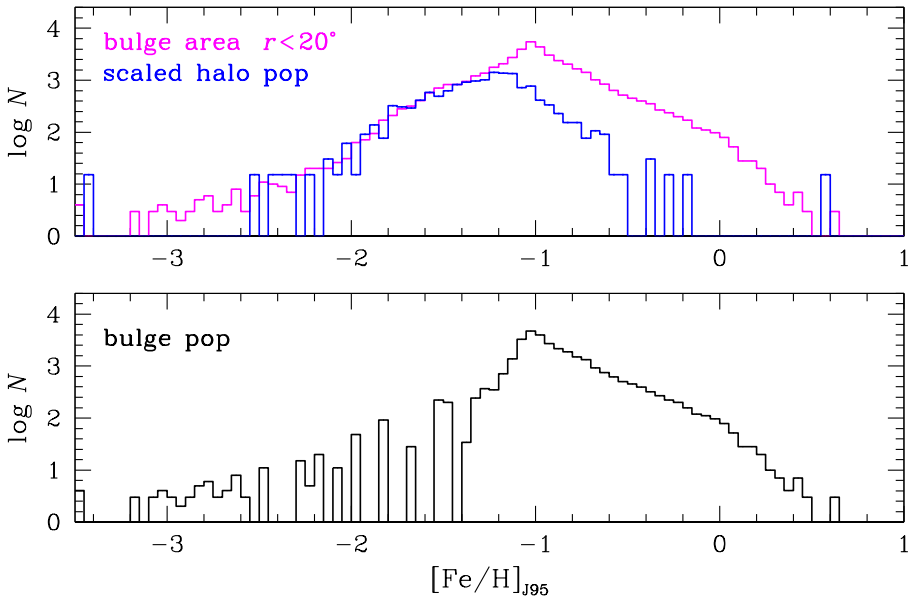

Fig. 4. Extraction of the metallicity profile for the bulge population by subtraction of the halo profile scaled to the bulge profile. In the whole bulge area, about 32% of RR Lyr stars are halo interlopers.

In the lower panel of Fig. 3, we present metallicity histograms for the three nearby irregular galaxies observed in the OGLE project: LMC, SMC, and Sgr dSph. For both Magellanic Clouds the OGLE collection is complete, while the disrupted Sgr dSph galaxy has only its core covered. The metallicity distributions for LMC, SMC, and Sgr dSph reach their maxima at about −1.3, −1.5, and −1.2 dex, respectively.

In the top three panels of Fig. 5, we compare normalized distributions for the nearby galaxies with the distribution for the Galactic halo. Sgr dSph seems to have the most similar metallicity distribution to the one of the halo. In the bottom panel of Fig. 5, we present the result of a simple experiment. We mixed RR Lyr samples from the three galaxies in equal proportion and normalized the obtained mixture to the halo. Such artificial population has an even more similar profile to the one of the halo. This experiment shows that the entire Galactic halo might be composed of stars from the accreted galaxies.

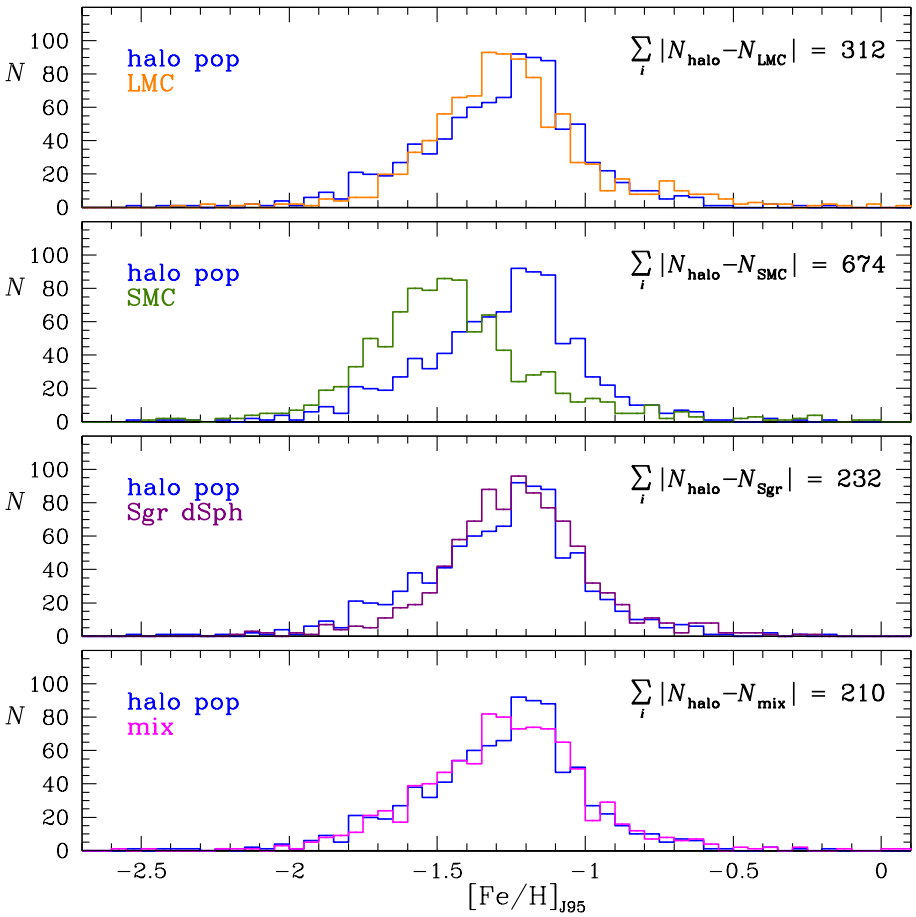

Fig. 5. Comparison between the metallicity distribution for the Milky Way's halo (blue histogram in all panels) with distributions normalized to the same number of stars for LMC, SMC, and disrupted Sgr dSph galaxy (three panels from the top) and for a mixture of equal number of stars from these three nearby galaxies (bottom panel). The latter distribution is the most similar to the halo distribution. It has the lowest sum of deviations calculated over the metallicity bins. This experiment suggests that the whole Milky Way's halo is formed from infalling material.

4 Period–amplitude diagrams

In Figs. 6 and 7, we present period–(I-band)amplitude diagrams (Bailey diagrams) for the inner bulge, outer bulge, disk area, and halo. For a transparent view, we plot only bulge variables with a small scatter around the light curve fit ($\sigma < 0.02$ mag), or stars without the Blazhko effect. In the case of less numerous disk and halo samples, we show all detected RRab stars. The presence of two adjacent sequences in the Bailey diagram, A and B, was discovered in the OGLE data for the inner bulge by Pietrukowicz *et al.* (2015). Here, we report that such a double sequence continues to the outer bulge. This result indicates that there are no major chemical differences between the inner bulge and the outer one.

Fig. 8 shows histograms in log$P$ for RRab stars from five Milky Way sections counted along the sequences in the I-band amplitude range 0.25–0.35 mag as marked in Figs. 6 and 7. This was done the same way as in Pietrukowicz *et*

al. (2015). Sequence A weakens with the increasing distance from the Galactic center. Outside the bulge, this sequence does not exist. In the Bailey diagram, we can see that sequence B is more blurred in the outer bulge than in the inner one. In Fig. 8, we find that halo and disk sequences peak at slightly higher period than sequence B. With the increasing distance from the center, the fraction of contributing halo stars increases and widens the sequence around $\log P \approx -0.2$.

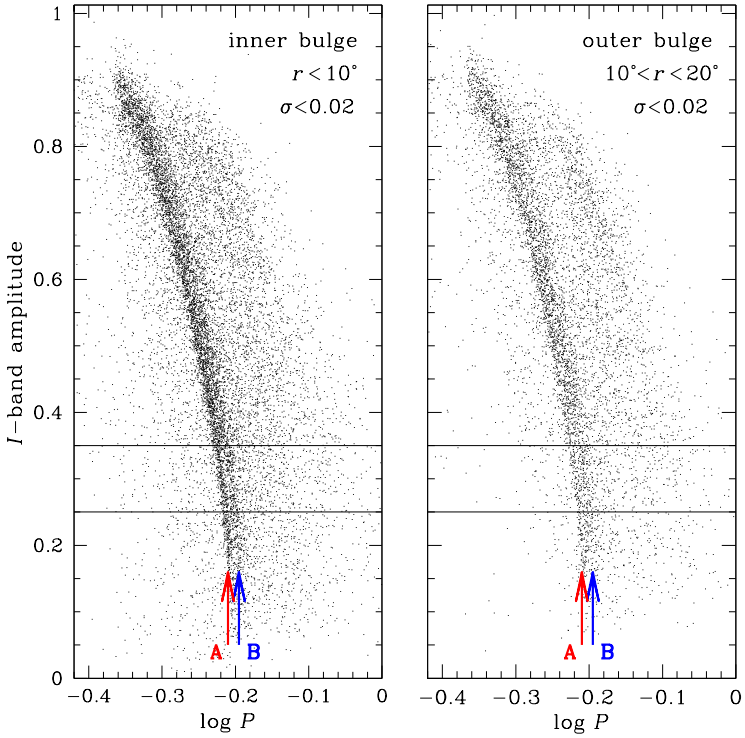

Fig. 6. Period-amplitude diagrams for the inner bulge (left panel) and outer bulge area (right panel). Two major bulge sequences, A and B, are marked. Horizontal lines denote the amplitude range used to count stars along the sequences (see Fig. 8). Only non-Blazhko RRab stars are plotted (with the scatter around the fit to the light curve $\sigma < 0.02$ mag).

In Fig. 9, we demonstrate that the old bulge cannot be treated as an inner extension of the halo or, more precisely, that the bulge sequence B is not an extension of the halo Oosterhoff group I (OoI). In the period–amplitude diagrams for the inner bulge, outer bulge, disk area, and halo, we draw curved stripes along the major sequence. The analyzed stripes are of the same size, limited by two fourth-order polynomials and amplitudes of 0.05 and 0.85 mag. Metallicity profiles for stars from the major sequence of the bulge, disk, and halo have different shapes and ranges. In particular, the bulge and halo populations are very distinct from each other.

5 Analysis of Old Populations in the Disk Area

RR Lyr stars in the observed disk area ($r > 30°$) belong to the halo and old disk populations. It is impossible to separate the stars based on photometry only. In Fig. 10, however, we make an attempt to extract the old disk population metallicity profile by scaling and subtracting the halo profile from the profile for the observed disk area. The scaling factor was found by minimizing the

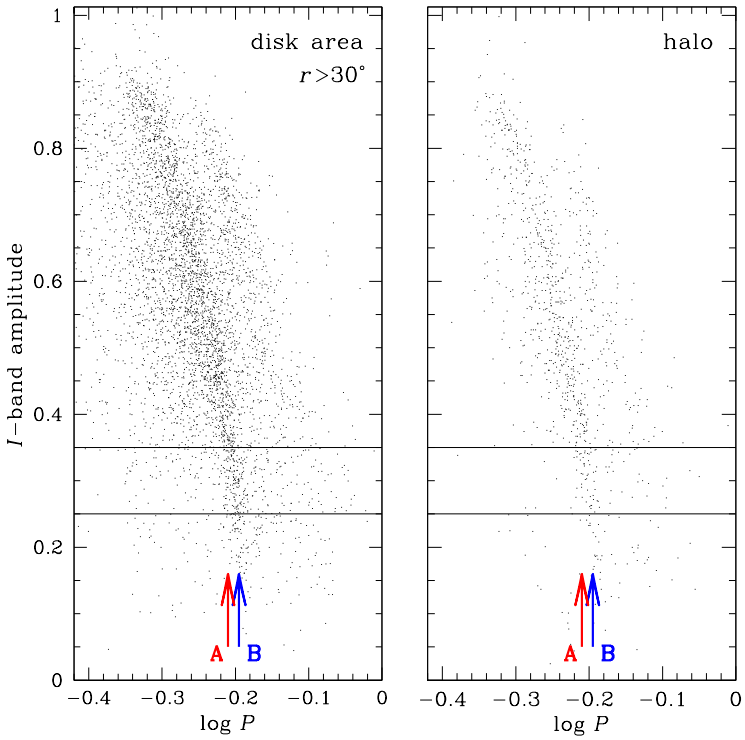

Fig. 7. Period-amplitude diagrams for the Galactic disk (left panel) and halo (right panel). Locations of the bulge sequences A and B are indicated.

difference between the metal-poor sides of the two distributions, for $[\mathrm{Fe/H}]_{\mathrm{J95}} \leq -1.2$ dex. The result is affected by the small number statistics. The true maximum of the disk population is at about -0.6 dex and the boundary value between the disk and the halo is located at -0.8 dex.

In Fig. 11, we draw separate maps for 2992 metal-poor ($[\mathrm{Fe/H}] < -0.8$ dex) and 961 metal-rich ($[\mathrm{Fe/H}] > -0.8$ dex) RRab stars. We present solely stars with Galactic longitude $l < -30°$ because the area closer to the bulge is contaminated with stars from that component. In the disk area, the fraction of metal-rich to metal-poor stars is about one-third and it slightly decreases with the increasing angular distance from the Galactic center (see bottom panel in Fig. 11). This result is reliable for $l > -110°$, where the observed area is symmetric with respect to the Galactic plane and the density of stars is large enough.

Fig. 12 shows number histograms for the metal-poor and metal-rich samples as functions of the Galactic latitude and its absolute value. We limited the sample to the range $-30° > l > -110°$. There is a small local peak at $b \approx -3°$. This is rather a serendipitous arrangement of stars emerging from clouds of dust than a real stream. The distribution of RR Lyr stars seems to be symmetric with respect to the Galactic plane. We do not see a structure similar to the Galactic warp in young populations (*e.g.*, classical Cepheids, Skowron *et al.* 2019). The histogram as a function of $|b|$ shows that the metal-poor and metal-rich RRab stars have different latitudinal distributions. When the metal-rich group gets less abundant beyond $|b| \approx 3°$, the number of metal-poor stars still increases. It is evident that the metal-rich group corresponds to the old (thick) disk and the metal-poor one belongs to the Galactic halo.

We tried to find possible relations between the Galactic coordinates, kine-

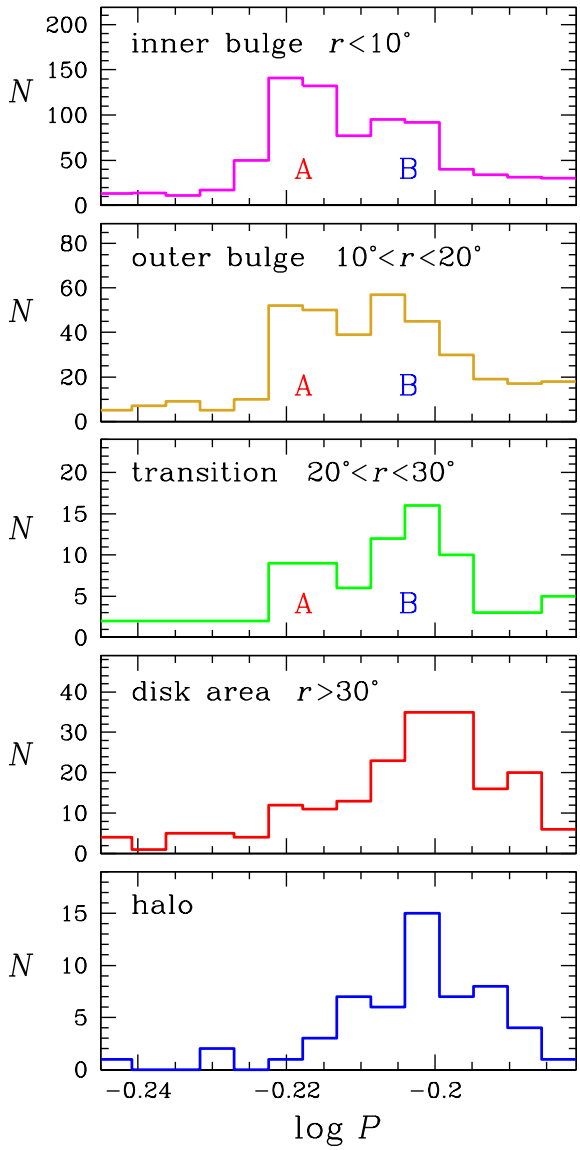

Fig. 8. Number histograms of RRab stars in the I-band amplitude range 0.25–0.35 mag in various directions of the Milky Way. Two peaks corresponding to the sequences A and B are clearly seen in the bulge area.

matics and iron abundance of RRab stars in the disk area. We cross-matched our disk sample with the *Gaia* DR2 source catalog (Gaia Collaboration *et al.* 2018). This was done for 4325 stars with $|l| > 30°$ and derived photometric metallicities. We adopted a matching radius of $0\farcs4$. For further investigation only stars without duplicates and stars with *Renormalised Unit Weight Error* RUWE<1.4 providing reliable astrometric solution were accepted. Almost 97% of the sources passed these criteria. In the next step, we transformed proper motions of 4187 stars from equatorial to Galactic system using equations given in Poleski (2013).

Fig. 13 presents distributions of median proper motions along the Galactic longitude (μ_l) and latitude (μ_b) determined in seven 20°-wide bins in the range

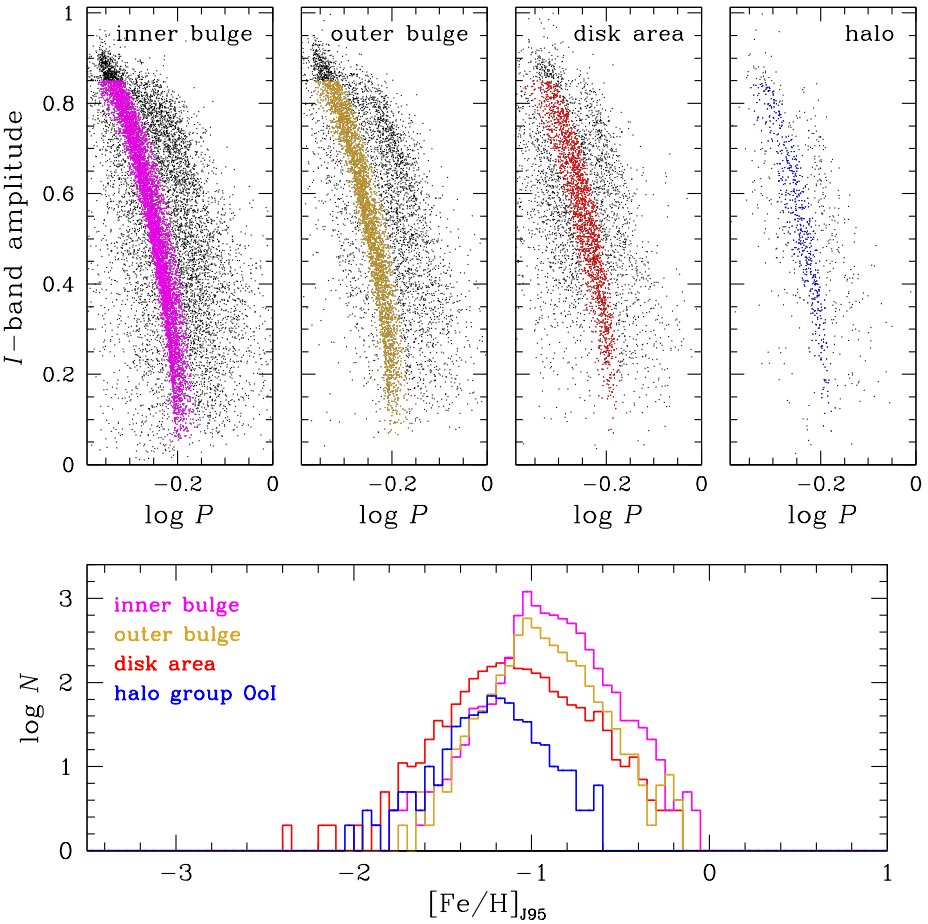

Fig. 9. Metallicity distributions (lower panel) for RRab stars along the major sequence in the period-amplitude diagram in four observed directions in the Milky Way (upper panels). The analyzed section in the Bailey diagram is the same in all Milky Way directions. Note that the metallicity distributions for the Galactic bulge, disk, and halo are different from each other.

$-30° > l > -170°$ and one bin for $+40° > l > +30°$. The distribution of the longitudinal proper motions forms a sinusoid. This is in agreement with the situation in which the Sun orbits the Galactic center in a kinematically hot halo. The obtained latitudinal proper motions are negative for the whole observed disk area with a mean value of -0.17 ± 0.02 mas/yr. The offset seems to result from the motion of the Sun toward the north Galactic pole with respect to the local standard of rest (LSR).

In Fig. 14, we show distributions of the latitudinal proper motions and their dispersion as a function of metallicity. We limit the plot to the area $-30° > l > -110°$ which is symmetric with respect to the Galactic plane. The median value of μ_b decreases slightly with the increasing iron abundance. In agreement with our expectations, the dispersion σ_{μ_b} drops with the increasing metallicity. Surprisingly, there is an outlying value at $[\mathrm{Fe/H}]_{\mathrm{J95}} = -1.0$ dex.

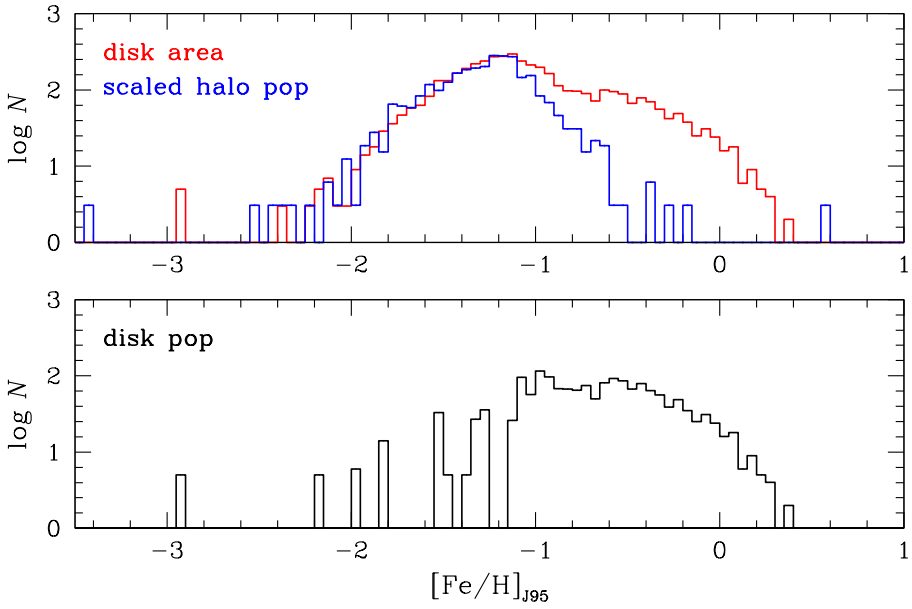

Fig. 10. Extraction of the metallicity distribution for the disk population from the sample of RRab stars observed in the disk area by subtraction of the halo population profile. The metallicity of the disk population spreads roughly from −1.2 to +0.3 dex with the true maximum value at about −0.6 dex.

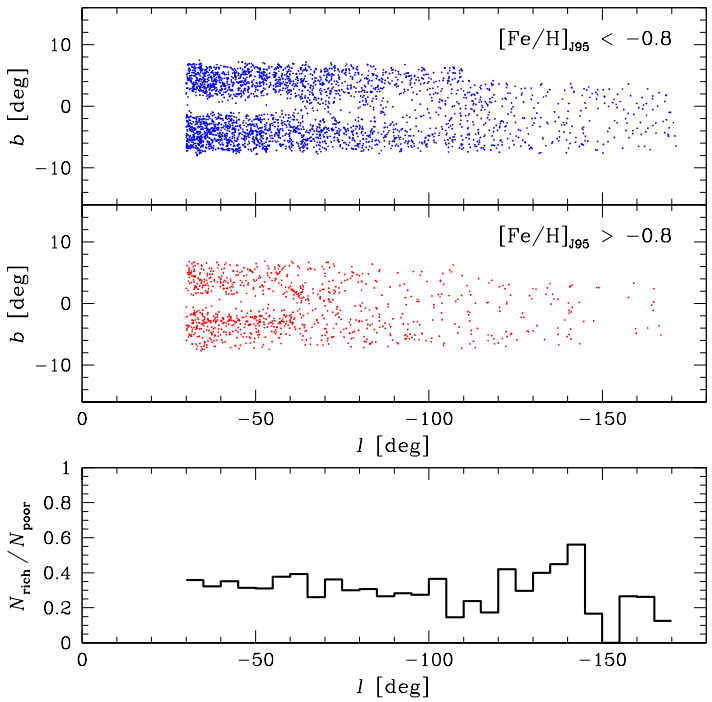

Fig. 11. Distribution of metal-poor (upper panel) and metal-rich RRab stars (middle panel) detected in the disk area. Lower panel: proportion of the stars as a function of Galactic longitude.

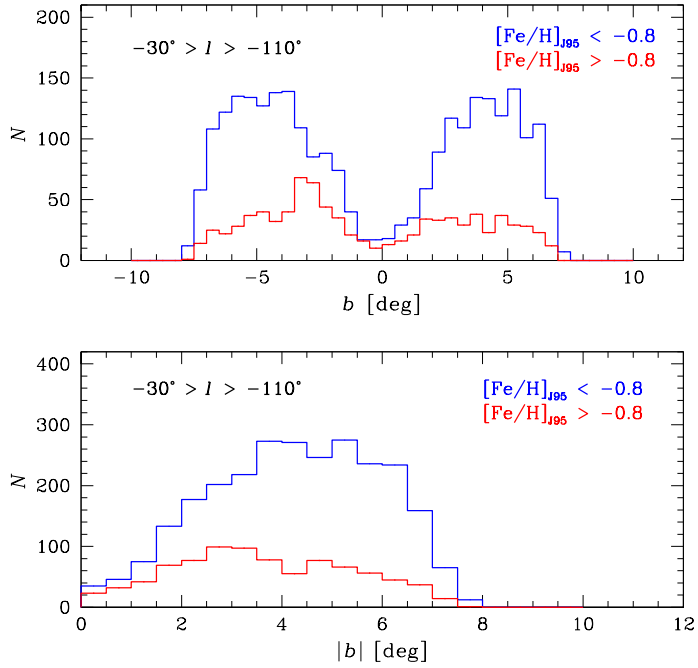

Fig. 12. Number histograms of metal-poor (blue) and metal-rich RRab stars (red) along the disk as a function of b (upper panel) and $|b|$ (lower panel). Completeness of the OGLE sample drops beyond $|b| \approx 6°$ due to the boundary of the observed footprint. Note that the number of metal-rich stars decreases closer to the Galactic plane than the metal-poor ones. This suggests that the former stars belong to the old disk population while the latter ones to the halo population.

6 Conclusion

We used the largest available homogeneous collection of Galactic RRab stars, the OGLE collection, to describe ancient stellar populations of the Milky Way based on photometric metallicity. From the metallicity distributions we concluded that there are solely three old components: the Galactic halo, Galactic bulge, and Galactic disk. A comparison of RR Lyr stars from the inner and outer bulge indicates that the entire old bulge is rather chemically homogeneous. The distributions of the inner and outer parts have a very similar shape and both peak at $[\mathrm{Fe/H}]_{\mathrm{J95}} \approx -1.0$ dex. We reported the presence of two adjacent sequences in the period–amplitude diagram, or populations A and B, also in the outer bulge. From the shape of the metallicity distributions we inferred that halo stars are found inside the bulge. About one-third of the RR Lyr stars in the bulge area, within 20° from the center, belong to the Galactic halo. This fraction drops to a quarter within 10°. Our result is consistent with expectations and the kinematic study of nearly 2800 bulge RR Lyr stars conducted by Kunder *et al.* (2020), who found that 25% of the variables are halo interlopers. Our experiment with mixing LMC, SMC, and Sgr dSph RR Lyr populations in equal proportions may suggest that the entire Milky Way's halo is formed from infalling dwarf galaxies, as we obtained a very similar metallicity distribution of the mixed populations to the one of the halo. The distribution for RR Lyr variables from the disk area has two peaks: one at $[\mathrm{Fe/H}]_{\mathrm{J95}} \approx -1.2$ dex corresponding to the halo component and the other one at $[\mathrm{Fe/H}]_{\mathrm{J95}} \approx -0.6$

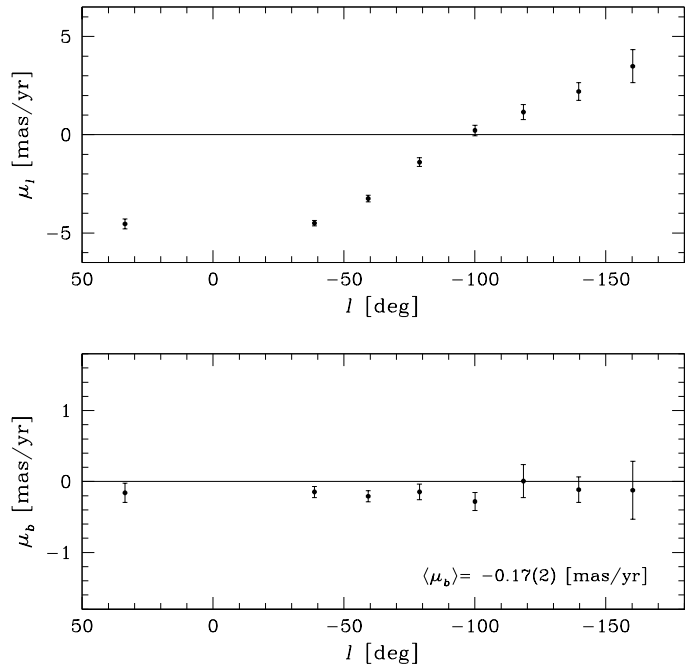

Fig. 13. Longitudinal (upper panel) and latitudinal proper motions (lower panel) of the disk RRab stars in the function of Galactic longitude. The observed sinusoidal trend in μ_l is consistent with the Sun orbiting the Milky Way's center in a kinematically hot halo. The value of μ_b is negative along practically the whole observed disk. This likely stems from the vertical motion of the Sun with respect to the local standard of rest.

dex corresponding to the disk component. The two components have different vertical number distributions. We thus confirmed that the disk population represented by RR Lyr stars exist, which has been implied based on several times smaller samples (*e.g.*, Kinemuchi *et al.* 2006, Mateu and Vivas 2018, Prudil *et al.* 2020). The spatial distribution of RR Lyr stars is symmetric with respect to the Galactic plane and no warp in the old disk population is seen. There is no evidence for the presence of multiple (more than two) components in the metallicity distribution for RRab stars in the disk area as found from near-infrared observations by Dékány *et al.* (2018). On-going spectroscopic and astrometric surveys (such as BRAVA-RR, APOGEE, *Gaia*) will provide more precise information on chemical composition and kinematics of the OGLE RR Lyr stars, which should allow for more detailed conclusions on the Milky Way's old populations.

Acknowledgments. We thank OGLE observers for their contribution to the collection of the photometric data over the years. The OGLE project has received funding from the National Science Centre, Poland, grant MAESTRO 2014/14/A/ST9/00121 to A.U. This work has been supported by the National Science Centre, Poland, grants OPUS 2016/23/B/ST9/00655 to P.P. and MAESTRO 2016/22/A/ST9/00009 to I.S. In this research, we used data from the European Space Agency (ESA) mission *Gaia*, processed by the *Gaia* Data Processing and Analysis Consortium (DPAC). Funding for the DPAC has been provided by national institutions, in particular the institutions participating in

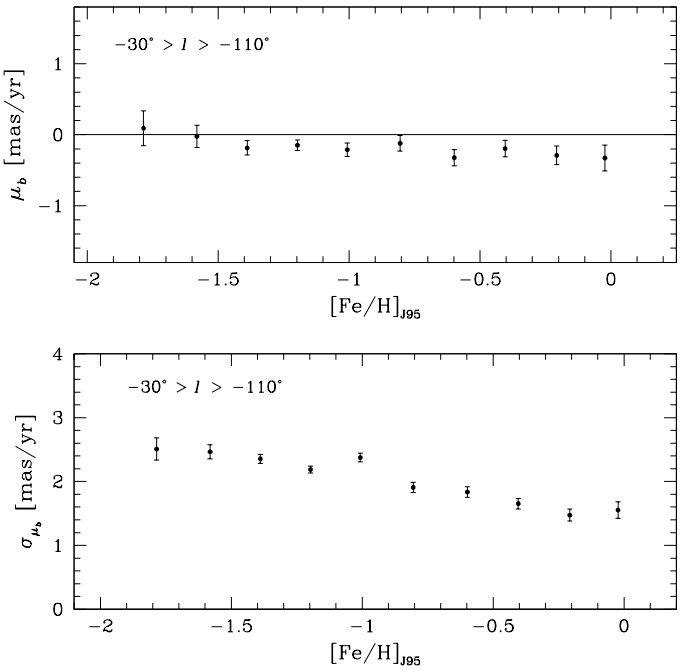

Fig. 14. Latitudinal proper motion (upper panel) and its dispersion (lower panel) as a function of metallicity for RRab stars from the Galactic disk area with $-30° > l > -110°$. Note that σ_{μ_b} decreases with the increasing metal content except for a significant bump around $[\mathrm{Fe/H}]_{\mathrm{J95}} = -1.0$ dex.

the *Gaia* Multilateral Agreement.

REFERENCES

Alcock, C. *et al.* 1998, *Astrophys. J.*, **492**, 190.
Belokurov, V. *et al.* 2018, *MNRAS*, **477**, 1472.
Braga, V.F. *et al.* 2015, *Astrophys. J.*, **799**, 165.
Braga, V.F. *et al.* 2016, *Astron. J.*, **152**, 170.
Clement, C.M. *et al.* 2001, *Astron. J.*, **122**, 2587.
Cusano, F. *et al.* 2017, *Astrophys. J.*, **851**, 9.
Dékány, I. *et al.* 2013, *Astrophys. J. Letters*, **776**, 19.
Dékány, I. *et al.* 2018, *Astrophys. J.*, **857**, 54.
Feuchtinger, M.U. 1999, *Astron. Astrophys.*, **351**, 103.
Fiorentino, G. *et al.* 2015, *Astrophys. J. Letters*, **798**, 12.
Fiorentino, G. *et al.* 2017, *Astron. Astrophys.*, **599**, A125.
Gaia Collaboration, Brown A.G.A. *et al.* 2018, *Astron. Astrophys.*, **616**, A1.
Jacyszyn-Dobrzeniecka, A.M. *et al.* 2017, *Acta Astron.*, **67**, 1.
Jeon, Y.-B., Ngeow, C.-C., and Nemec, J.M. 2014, *IAU Symp.*, **301**, 427.
Jurcsik, J. 1995, *Acta Astron.*, **45**, 653.
Jurcsik, J., and Kovács, G. 1996, *Astron. Astrophys.*, **312**, 111.
Kinemuchi, K. *et al.* 2006, *Astron. J.*, **132**, 1202.
Kovács, G., and Zsoldos, E. 1995, *Astron. Astrophys.*, **293**, L57.
Kunder, A. *et al.* 2013, *Astron. J.*, **146**, 119.
Kunder, A. *et al.* 2020, *Astron. J.*, **159**, 270.
Majaess, D. *et al.* 2018, *Astrophys. J. Suppl. Ser.*, **363**, 127.
Marconi, M. *et al.* 2015, *Astrophys. J.*, **808**, 50.
Martínez-Vázquez, C.E. *et al.* 2016, *MNRAS*, **462**, 4349.
Martínez-Vázquez, C.E. *et al.* 2017, *Astrophys. J.*, **850**, 137.
Mateu, C., and Vivas, A.K. 2018, *MNRAS*, **479**, 211.
Nemec, J.M., *et al.* 2013, *Astrophys. J.*, **773**, 181.

Pietrukowicz, P. *et al.* 2012, *Astrophys. J.*, **750**, 169.
Pietrukowicz, P. *et al.* 2015, *Astrophys. J.*, **811**, 113.
Prudil, Z. *et al.* 2019, *MNRAS*, **484**, 4833.
Prudil, Z. *et al.* 2020, *MNRAS*, **492**, 3408.
Poleski, R. 2013, , , arXiv:1306.2945.
Sarajedini, A. *et al.* 2012, *MNRAS*, **425**, 1459.
Skowron, D.M. *et al.* 2016, *Acta Astron.*, **66**, 269.
Skowron, D.M. *et al.* 2019, *Science*, **365**, 478.
Smolec, R. 2005, *Acta Astron.*, **55**, 59.
Soszyński, I. *et al.* 2014, *Acta Astron.*, **64**, 177.
Soszyński, I. *et al.* 2019a, *Acta Astron.*, **69**, 87.
Soszyński, I. *et al.* 2019b, *Acta Astron.*, **69**, 321.
Szczygieł, D.M., Pojmański, G., and Pilecki, B. 2009, *Acta Astron.*, **59**, 137.
Torrealba, G. *et al.* 2015, *MNRAS*, **446**, 2251.
Tsapras, Y. *et al.* 2017, *MNRAS*, **465**, 2489.
Udalski, A., Szymański, M.K., and Szymański, G. 2015, *Acta Astron.*, **65**, 1.
Woźniak, P.R. 2000, *Acta Astron.*, **50**, 421.
Zinn, R. *et al.* 2014, *Astrophys. J.*, **781**, 22.